IEEE Access
Multidisciplinary | Rapid Review | Open Access Journal

Received September 5, 2018, accepted September 19, 2018, date of publication October 4, 2018, date of current version October 29, 2018.

Digital Object Identifier 10.1109/ACCESS.2018.2873784

Motion Analysis and Compensation Method for Random Stepped Frequency Radar Using the Pseudorandom Code

ZHIKUN LIAO, JIEMIN HU, DAWEI LU, (Member, IEEE), AND JUN ZHANG
ATR Laboratory, National University of Defense Technology, Changsha 410073, China
Corresponding author: Zhikun Liao (lzkun2008@yeah.net)

This work was supported by the National Natural Science Foundation of China under Grant 61401479.

ABSTRACT To address the defocusing problem faced by random stepped frequency (RSF) radars, this paper presents a complementary code cancellation (CCC) method to estimate the target velocity and achieve motion compensation. The proposed CCC method is capable of eliminating the coupling effect between range profile and target velocity. In this paper, we first give a block diagram of RSF radar modulated by the M-sequence-generated pseudorandom code, and introduce the baseband sampling echo model of moving target. Then, the velocity estimation accuracy is derived to show the sensitivity of high-resolution range profile to target velocity. Subsequently, the CCC method is proposed and also investigated in the application of multi-target scenario. Performance analyses demonstrate that the proposed method can satisfy the estimation accuracy requirement and improve the signal to noise ratio by the velocity accumulation. Finally, simulations show that the method is effective and more computationally efficient than the existing popular methods.

INDEX TERMS Random stepped frequency radar, high-resolution range profile, M-sequence, defocusing problem, velocity tolerance, motion compensation.

I. INTRODUCTION

Linear stepped frequency (LSF) signal has been widely utilized in the high-resolution range profile (HRRP) radars [1]–[4]. Since the modulated frequencies of LSF radar are distributed step-by-step over the specific bandwidth, the baseband echoes can be treated as the uniform sampling signals in frequency domain. Its range compression can be easily achieved by performing the inverse fast Fourier transform (IFFT) on the baseband echoes. The range resolution is determined by the synthetic bandwidth [5]. However, the compressed range profile is ambiguous, and the range-Doppler ambiguity function of transmitted waveform is a periodical slant ridge [6]. It implies that the deviation of velocity compensation causes the circular shifts of the HRRP, which is the shift coupling effect between the range profile and estimated velocity of LSF radar.

To suppress the range ambiguity, in the literature [7]–[9], random hopped frequency (RHF) radar is introduced as a discrete version of noise radar. The transmitted waveform of noise radar is continuously modulated by the random noise [10]–[12]. The modulated frequencies of the monotone transmitted waveform of RHF radars [8] are taken from the noise. Since the modulated frequencies are randomly distributed, the coupling effect of range profile and estimated velocity in RHF radars are different from LSF radars. Instead, the RHF radar has an ideal thumbtack range-Doppler ambiguity function. As the modulated frequencies are random, the HRRP of RHF radar is synthesized by correlation processing [13] or compressive sensing [14]. But, both methods have high computation complexities.

Random stepped frequency (RSF) radar modulated by the pseudorandom code is capable of overcoming this contradiction. The pseudorandom code is a unique integer sequence, such as Costas code [15], [16] or Chaos code using Bernoulli mapping [17]. Its range compression can also be achieved by IFFT processing on the sorted baseband echoes to significantly reduce the computation complexities. Meanwhile, the disordered modulated frequencies also make it possess the thumbtack ambiguity function.

The thumbtack ambiguity function improves the measurement accuracies in both range and Doppler dimensions, but it also indicates that the HRRP is sensitive to the Doppler frequency. A small radial velocity or compensation mismatch may cause serious destruction on the synthetic HRRP, i.e., the

defocusing problem, which was briefly discussed in [18]. Therefore, the precise estimation and compensation of target velocity is required before synthesizing the focused HRRP for RSF radars. Generally, motion compensation is achieved in two steps [19]: range alignment and phase compensation. Different range alignment approaches, for instance, locking the first strong peak of each echo onto a specific range bin, envelope correlation or the spectral domain phase difference [20], have been introduced. They can be transplanted into the RSF radars.

For the second step, some solutions can be applied in HRRP radars. They are cross-correlation between two adjacent pulse-trains (CC-TAP) [21]–[23], the Hough transform on tracked strong scatterers (HT-TSS) [19], a bank of Doppler filters (DFs) [24], minimum waveform entropy (MWE) [18] [25]–[27], the range velocity iterative alternating project (RV-IAP) [28], time-frequency distribution (TFD) [29]–[31], Radon-fractional Fourier transform (RFRFT) [32], [33], and Radon-Lv's distribution (RLVD) [34], [35]. The CC-TAP method does not have sufficient velocity estimation accuracy. In RSF radars, highlighting the strong moving scatterers in the HRRP before velocity estimation is difficult since the HRRP is dispersed by the velocity. As a result, the HT-TSS method cannot be adopted in RSF radars. The DFs and MWE methods are implemented by enumerating all possible velocities via placing parallel hardware resources and minimizing cost functions, respectively. Both methods consume a lot of calculations. Similarly, the RV-IAP algorithm requires an ergodic search from 1 to the target number, and each iterative step contains the matrix inversion loops until converging. It also requires numerous calculations. Furthermore, the RV-IAP algorithm needs the target number as prior knowledge. For LSF radars, the baseband echoes with constant velocity or constant acceleration after time-frequency transforming are distributed as a ridge along straight line or quadratic curve. Then, detecting the intercept and slope of the line or the coefficients of the quadratic curve is capable of obtaining the range, velocity and acceleration of target. However, the TFD algorithm is not suitable for RSF radars, for the echoes after time-frequency transforming are stochastic all over the plane. The RFRFT and RLVD methods achieve the long-time coherent integration of the pulse-compressed echo signals to improve the detection ability of a weak maneuvering target for linear frequency modulated (LFM) radars. The target's energy is coherently accumulated as a peak in the time-range plane to estimate the range, velocity and acceleration via both methods. But, the pulse compression cannot be performed prior to the motion parameter estimation in RSF radars.

In order to solve the defocusing problem for RSF radars, an efficient velocity estimation method, called complementary code cancellation (CCC), is proposed in this paper. The paper is organized as follows. Firstly, the block diagram of RSF radar modulated by the M-sequence-generated pseudorandom code is exhibited in Sec. II. Then, the baseband echo model is introduced in Sec. III. In Sec. IV, the velocity tolerance is derived to indicate the motion compensation accuracy requirement of RSF radar. Subsequently, the CCC method to achieve the motion compensation is presented in Sec. V. Moreover, the proposed method is simulated in the multi-target scenario and compared with the existing method in Sec. VI. Finally, Sec. VII provides the conclusions.

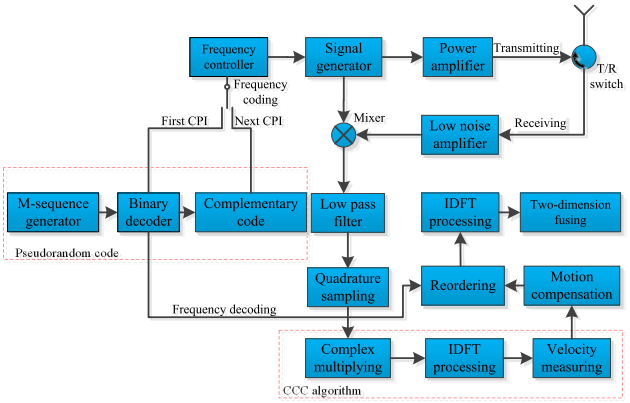

FIGURE 1. A block diagram of RSF radar system using the M-sequence as pseudorandom code source.

II. THE BLOCK DIAGRAM OF RSF RADAR

The block diagram of RSF radar using M-sequence as pseudorandom code source is presented in Figure 1.

The pseudorandom code is generated by decoding the binary flow from the M-sequence generator. Then, the code is split into two channels: one is to drive the frequency controller to modulate the transmitted waveform, and the other is to reorder the compensated baseband echoes in the coherent receiver. The frequency controller produces the modulated frequency for current pulse through an alternative switch to select the primitive code or complementary code. The waveform is upconverted with the carrier frequency in the signal generator module and is transmitted after amplified in the power amplifier module. The received echoes are amplified by the low-noise amplifier, and then downconverted to baseband with the transmitted waveform as local oscillator (LO). After the low pass filtering and quadrature sampling, the CCC algorithm is performed to estimate the target velocity before synthesizing the HRRP. The procedure of CCC algorithm is contained in the red-dashed box at the bottom of the diagram. The estimated velocity is used to compensate echo phase. Then, the focused HRRP can be synthesized by reordering and IDFT processing on the compensated echoes [36].

M-sequence has been widely utilized in the field of radar and communication to produce quasi-Gaussian white noise. The code generated from M-sequence maintains the random characteristics. The number of pulses in a pulse-train is always set to the integer power of 2 in RSF radars, which is the same as the length of M-sequence. But, if the number of pulses is not exactly equal to the integer power of 2, this method still works. A few comparator circuits shall be added

TABLE 1. Parameter descriptions.

Parameter	Description
c	The propagation speed of light
N	The number of pulses in a train
T	Pulse duration
T_r	Pulse repetition interval (PRI)
T_{CPI}	Coherent processing interval (CPI)
f_0	Carrier frequency
Δf	Frequency step interval
B	Synthetic bandwidth
σ	Target backscatter coefficient
c_n	Frequency modulation coefficient
R_0	Radial range between the radar and target
V_0	Relative radial velocity
$\hat{x}$	An inverse angle over x is used to indicate the complementary form of x.
$\tilde{x}$	A wave symbol over x is used to to indicate the reordered result of x.

after the binary decode module to determine whether the current code is less than the number of pulses. The code is preserved, if it is less than the number of pulses. Otherwise, the code is skipped.

III. ECHO SIGNAL MODEL OF MOVING TARGET

Consider a radar using the RSF waveform with a train of N coherent pulses whose monotone frequencies randomly jump within the given bandwidth. The main parameters presented in the paper are listed in Table 1.

The complex form of transmitted waveform is written as

$$s(t) = \sum_{n=0}^{N-1} u_n(t - nT_r) \exp(j2\pi f_0 t) \tag{1}$$

where $u_n(t)$ is the envelope function

$$u_n(t) = rect\left(\frac{t}{T}\right) \exp(j2\pi c_n \Delta f t). \tag{2}$$

In the envelope function, $rect(x)$ is a unit rectangle function. When $0 \le x \le 1$, $rect(x)$ is equal to 1; otherwise, it is zero. Coefficient $c_n \in \{1, 2, \cdots, N\}$ is the pseudorandom code generated from M-sequence, satisfying $c_n \neq c_m$ when $n \neq m$.

Given a point target at the initial radial range R_0 with the radial velocity V_0 moving away from the radar, the real-time range between radar and target is

$$r(t) = R_0 + V_0 t. \tag{3}$$

The echo from the illuminated target is the scaled and time-delayed version of transmitted signal. That is

$$s_r(t) = \sigma s(t - \tau) \tag{4}$$

where $\tau(t) = 2r(t)/c$ denotes the echo delay.

The echo is first coherently demodulated with the transmitted waveform as LO. After the low pass filtering, the echo is transferred to baseband. That is

$$s_{rb}(t) = \sigma \exp(-j2\pi (f_0 + c_n \Delta f) \tau(t)). \tag{5}$$

Subsequently, the baseband echo is sampled at the moment $t = nT_r + lT_s$. T_s is the sampling interval which is usually equal to T in RSF radars. It is assumed that the target does not move across range bins. The sampling outputs form a data matrix whose row and column indices indicate the pulse number n and range bin l, respectively. However, there is only one column in matrix containing the sampling echoes of point target.

$$y_r[n, l_0] = \sigma \exp\left(-j\frac{4\pi}{c}(f_0 + c_n \Delta f)(R_0 + V_0 n T_r)\right) + w_n \tag{6}$$

where $l_0 = [\![2R_0/(cT_s)]\!]$ is the range bin of the target, $[\![\ ]\!]$ is the rounding operator, and w_n is the zero-mean and ε-variance additive white Gaussian noise (AWGN).

As Figure 1 show, the HRRP of point target is the IDFT result of its reordered sampling echo. It is assumed that $\tilde{y}_r[n, l_0]$ is the reordered version of sampling echo $y_r[n, l_0]$ according to the coefficient c_n. That is

$$\tilde{y}_r[n, l_0] = \sigma \exp\left(-j\frac{4\pi}{c}(f_0 + n\Delta f)(R_0 + V_0 \tilde{c}_n T_r)\right) + \tilde{w}_n. \tag{7}$$

Signal $\tilde{Y}_r[k, l_0]$ is the K-point IDFT of $\tilde{y}_r[n, l_0]$. Then, the HRRP of the target can be expressed as

$$P[r] = \left|\tilde{Y}_r\left[\left(\frac{2r}{c}\Delta f K\right)_K, l_0\right]\right|, \quad r \in [R_{l_0-1}, R_{l_0}] \tag{8}$$

where $(x)_K$ returns the remainder after x is divided by K, $R_{l_0-1} = (l_0 - 1) cT_s/2$ and $R_{l_0} = l_0 cT_s/2$ are the start and end range of the l_0th range bin, respectively. Due to the periodicity of IDFT, the range r is mapped to variable k and taken the remainder in Eq. (8).

IV. VELOCITY ESTIMATION ACCURACY

In RSF radars, target velocity will collapse its HRRP, called the the defocusing effect [18]. In this section, the velocity tolerance that does not induce the significant defocusing effect on the HRRP is introduced to indicate the motion compensation accuracy. At first, Figure 2 are given to illustrate the different reactions of HRRPs to the target velocities.

The HRRP of the stationary target, shown in the red lines, are the standard discrete $sinc(x) = \sin(x)/x$ function. However, when the target is moving, its HRRP peak gradually decays until completely submerged in the side-lobes. As Figure 2 shows, when target velocity $V_0 = 0.1$ m/s, the HRRP peak decays to 0.85 and the side-lobes become stochastic. But, the position of HRRP peak still reflects the target range R_0. If velocity continues to increase, the peak completely fades into side-lobes.

The peak is gradually attenuated. There is critical value that indicates the severity of HRRP peak attenuation. The velocity tolerance (VT) is introduced to identify the velocity that attenuates the HRRP peak by 3 dB. The HRRP of the target at the range of R_0 with the velocity of v is expressed

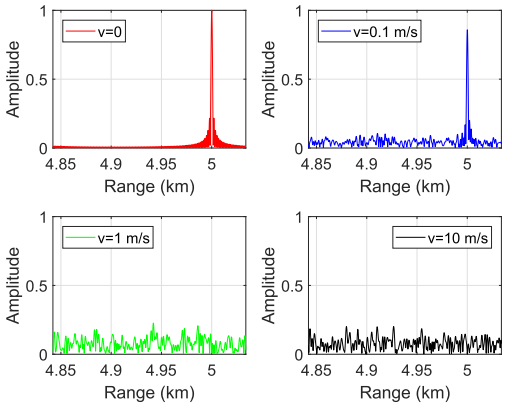

FIGURE 2. An example of RSF radar HRRP of four targets at the range of $R_0 = 5$ km with different velocities of 0, 0.1, 1 and 10 m/s *versus* the range in km. Radar parameters are carrier frequency $f_0 = 35$ GHz, synthetic bandwidth $B = 100$ MHz, $N = 128$, PRI $T_r = 100\,\mu s$ and pulse duration $T = 1\,\mu s$

as $P[r\,|R_0, v]$. Then, VT is the solution of following equation

$$20\log_{10}\frac{P[R_0\,|R_0, v]}{P[R_0\,|R_0, 0]} = -3. \tag{9}$$

Generally, the carrier frequency is much greater than the synthetic bandwidth $B = N\Delta f$, i.e., $f_0 \gg B \geq c_n\Delta f$. When V_0 is close to 0, the term $-4\pi n\Delta f V_0\tilde{c}_n T_r/c$ in the reordered echo can be neglected as a tiny phase noise. In order to acquire the VT more accurately, $-4\pi BV_0\tilde{c}_n T_r/2c$ is subtracted from the phase noise to halve the the absolute value of phase fluctuation. Substituting Eq. (8) into Eq. (9), VT can be approximated as the solution of the following equation

$$\left|\frac{\sin\left(2\pi\left(f_0 + B/2\right)vNT_r/c\right)}{N\sin\left(2\pi\left(f_0 + B/2\right)vT_r/c\right)}\right| = 10^{-3/20}. \tag{10}$$

Solving the equation, we can obtain

$$v_T = \frac{0.221c}{\left(f_0 + B/2\right)NT_r}. \tag{11}$$

Carrier frequency is always very large for the common radar frequency band, thus causing a quite small VT. For instance, a RSF radar working at L band with $T_{\mathrm{CPI}} = 5$ ms has a VT from 5 m/s to 10 m/s which is equivalent to the human walking speed. For another example, the VT of RSF radar with 35 GHz carrier frequency and 5 ms CPI is only 0.1465 m/s.

VT is a property of RSF radar to weigh its sensitivity of the HRRP to target velocity. If the target velocity does not exceed the VT, the synthetic HRRP is not significantly affected. Otherwise, the motion compensation is necessary to prevent the defocusing problem in HRRP. In other words, VT provides a accuracy criterion of motion compensation for RSF radars.

V. RSF RADAR MOTION COMPENSATION VIA CCC ALGORITHM

Target velocity always plays an important role in the synthesis processing of HRRP; specifically, its effect is manifested as the defocusing problem in RSF radars. The VT indicating the velocity compensation accuracy, is quite small due to the high radar carrier frequency. It implies that the HRRP of RSF radar is sensitive to target velocity. Therefore, before synthesizing the HRRP, the target velocity should be estimated and compensated with a high accuracy that is not less than VT. In this section, the complementary code cancellation method is proposed to achieve the velocity estimation for RSF radars.

A. CCC ALGORITHM

There is only one column of valid data in the echo matrix of point target. However, the target echo in Eq. (6) contains both range and velocity information. Consequently, the CCC algorithm is designed to utilize complementary pseudorandom codes to modulate the transmitted pulses in the adjacent CPIs. Then, the range and velocity in these two complementary matrices are separable.

1) ALGORITHM INTRODUCTION

At the transmitting terminal, the RSF waveform in Eq. (1) is adopted during the previous CPI. However, the waveform with the same other parameters but a different frequency modulation coefficient is transmitted in the succeeding CPI. The coefficients c_n and $\hat{c}_n$ in the adjacent CPIs satisfy the following complementary relationship

$$c_n + \hat{c}_{n+N} = N, \quad n = 0, 1, \cdots, N-1. \tag{12}$$

The envelope function $\hat{u}_n(t)$ in the succeeding CPI is

$$\hat{u}_n(t) = rect\left(\frac{t}{T}\right)\exp\left(j2\pi\hat{c}_n\Delta f t\right). \tag{13}$$

After the coherent demodulation and quadrature sampling, the baseband echoes of the moving point target in the succeeding CPI has a similar expression as Eq. (6)

$$\hat{y}_r[n, l_0] = \sigma\exp\left(-j\frac{4\pi}{c}\left(f_0 + \hat{c}_n\Delta f\right)\left(R_0 + V_0 nT_r\right)\right) + \hat{w}_n \tag{14}$$

where $n = N, N+1, \cdots, 2N-1$ and $\hat{w}_n$ is the same AWGN as w_n in the succeeding CPI.

Let $i = n - N$ and do not consider noise term temporarily

$$\hat{y}_r[i, l_0] = \sigma\exp\left(-j\frac{4\pi}{c}\left(f_0 + \hat{c}_{i+N}\Delta f\right)\left(R_0 + V_0\left(i+N\right)T_r\right)\right) \tag{15}$$

where $i = 0, 1, \cdots, N-1$.

The range terms in Eqs. (6) and (15) constitute a complementary pair. The changing range terms can be turn into a constant phase term by multiplying the sampling echoes of

the adjacent CPIs. Then, the remaining part is composed of the velocity terms except for the constant term. That is

$$\begin{aligned}\upsilon[n] &= y_r[n,l_0]\cdot\hat{y}_r[n,l_0]\\ &= \sigma^2\exp(-j\varphi_0)\exp\left(-j\frac{4\pi}{c}(2f_0+N\Delta f)V_0nT_r\right)\\ &\quad\cdot\exp\left(j\frac{4\pi}{c}c_n\Delta f V_0NT_r\right)\end{aligned} \tag{16}$$

where φ_0 contains all constant phases

$$\varphi_0 = \frac{4\pi}{c}\left[f_0(2R_0+V_0NT_r)+N\Delta f(R_0+V_0NT_r)\right]. \tag{17}$$

Except for the constant phase term, there are linear phase term and random phase term left in the multiplying result. The carrier frequency is much greater than synthetic bandwidth. If the random phase is less than $\pi/2$, the random phase term can be treated as a tiny noise interference. The velocity should satisfy

$$\max_n\left\{\frac{4\pi}{c}c_n\Delta f V_0NT_r\right\} \le \frac{\pi}{2} \Rightarrow V_0 \le \frac{c}{8N^2\Delta f T_r}. \tag{18}$$

The linear phase term plays the most important role in the fluctuation of multiplying result. The target velocity determines the discrete frequency of the linear phase term. Therefore, it is efficient to perform an IDFT processing on the multiplying output to accumulate the velocity profile. After using the absolute value of IDFT result, the range term is removed. When the target is not moving too fast or its velocity is coarsely pre-compensated, the Q-point IDFT result on the multiplying output can be approximated to

$$\begin{aligned}\Upsilon[q] &= \left|\mathcal{F}^{-1}\{\upsilon[n]\}\right|\\ &\approx \frac{\sigma^2}{N}\left|\frac{\sin\frac{\pi N}{Q}\left(q-\frac{2}{c}(2f_0+N\Delta f)V_0T_rQ\right)}{\sin\frac{\pi}{Q}\left(q-\frac{2}{c}(2f_0+N\Delta f)V_0T_rQ\right)}\right|.\end{aligned} \tag{19}$$

where $\mathcal{F}^{-1}$ denotes the IDFT processing. The velocity profile is also a discrete $sinc(x)$ function approximately. The target velocity can be obtained by traversing the IDFT result and addressing the index of its maximum value. Since the discrete signal has period spectrum, the detected velocity also possesses an unambiguous region.

Then, the target velocity can be estimated by executing a detection algorithm, e.g., constant false alarm rate (CFAR) detection, on the velocity profile. For the point target, the detection processing is to search the maximum value

$$\bar{q} = \arg\max_{1\le q\le Q}\{\Upsilon[q]\}. \tag{20}$$

The estimated velocity is

$$\bar{V}_0 = \frac{c\bar{q}}{2(2f_0+N\Delta f)T_rQ}. \tag{21}$$

Subsequently, the motion compensation factor can be generated with this estimated velocity $\bar{V}_0$ as

$$\bar{\sigma}_{\bar{V}_0}[n] = \exp\left(j\frac{4\pi}{c}(f_0+c_n\Delta f)\bar{V}_0nT_r\right). \tag{22}$$

Finally, the sampling echoes in the previous CPI in Eq. (6) is multiplied by the compensation factor; thus achieving the motion compensation. The focused HRRP in the current range bin is synthesized by performing an IDFT processing on the compensated echoes.

2) ALGORITHM DESCRIPTION

The CCC algorithm to estimate the target velocity is summarized in **Algorithm 1**.

Algorithm 1 The CCC Algorithm

Input: the echo matrices $y_r[n,l]$ and $\hat{y}_r[n,l]$ of the adjacent CPIs modulated by the complementary coefficients c_n and $\hat{c}_n$.

Output: the estimated target velocity $\bar{V}_0$

1: The corresponding elements of both matrices y_r and $\hat{y}_r$ are multiplied to generate υ.
2: **for** $l = 0$ to $L-1$ **do**
3: A Q-point IFFT processing is performed along the lth column of υ.
4: The velocity profile Υ is generated using the absolute value of IFFT result.
5: CFAR detection is executed on the lth column of velocity profile Υ to obtain the estimated velocity $\bar{V}_0$.
6: **end for**

The IFFT is a fast implementation algorithm for the IDFT processing. The butterfly structure of radix-2 or radix-4 can be used to implement the IFFT. **Algorithm 1** embodies the specific procedure of the CCC algorithm in the red-dashed box at the bottom of Figure 1. The detailed algorithm performance will be analyzed in the next subsection.

3) ALGORITHM ANALYSIS

The complementary codes produce a pair of orthogonal echo matrices to separate the target range and velocity. Since the accumulation time is doubled, the velocity resolution precision of CCC algorithm can be improved. According to Eq. (19), the 3 dB resolution is

$$\Delta v = \frac{0.442c}{(2f_0+N\Delta f)NT_r}. \tag{23}$$

The target velocity can be either positive or negative, corresponding to traveling away from or toward the radar. However, the definition of VT does not take the direction of target movement into account. In order to analyze the resolution performance, the VT should be multiplied by 2. The ratio between 3 dB resolution of the proposed method and doubled VT is

$$\Lambda(f_0) = \frac{\Delta v}{2v_T} = \frac{1}{2}. \tag{24}$$

It can be seen that the velocity resolution of the CCC algorithm is only half of the accuracy requirement of motion compensation. That is, the estimated velocity based on the CCC algorithm can sufficiently satisfy the requirements of

motion compensation to synthesize the focused HRRPs for RSF radars. Replacing v in Eq. (10) with the 3 dB resolution Δv, the attenuation of HRRP peak is about 0.92. It means that the signal loss caused by the estimation error of CCC algorithm is less than 0.71 dB.

Because of the periodicity of IDFT processing, the estimated velocity has an unambiguous interval. That is

$$Pv = \frac{c}{2\left(2f_0 + N\Delta f\right)T_r}. \tag{25}$$

The unambiguous velocity interval that is subject to the large carrier frequency, is not adequate to detect fast-moving targets. Once the target velocity exceeds the unambiguous interval, not only the ambiguous error would occur in the velocity profile, but also the velocity profile may be strongly disturbed by the random phase term. Therefore, a coarse motion compensation, e.g., using inertial navigation, is required to detect the fast-moving target in advance. The smaller one of unambiguous velocity interval and velocity threshold defined in Eq. (18) restricts the accuracy of coarse motion compensation.

The IDFT could be fast implemented by the radix-2 IFFT. When achieving the CCC algorithm, the number of complex multiplications in one range bin is

$$\eta\left(N\right) = N + \frac{Q}{2}\log_2 Q \tag{26}$$

where $Q = 2^{\lceil \log_2 N \rceil}$ is the IFFT length, and $\lceil\ \rceil$ denotes the ceil operator to round the element to the nearest integer towards infinity. The first N at the right-hand side of equal sign in Eq. (26) is introduced during the complex multiplication of two sampling echoes in the adjacent CPIs. While, the remaining part related to Q is caused by the IFFT processing. The computational complexity of the proposed algorithm is $O\left(N\log_2 N\right)$ which is significantly reduced compared with existing methods.

According to the sampling echo in Eq. (6), the input signal-to-noise ratio (SNR) of the CCC algorithm is

$$\zeta_i = \frac{\sigma^2}{\varepsilon}. \tag{27}$$

Taking the noise w_n into the algorithm, the output SNR can be obtained as

$$\zeta_o = \frac{N\sigma^4}{2\sigma^2\varepsilon + \varepsilon^2} = N\frac{{\zeta_i}^2}{2\zeta_i + 1}. \tag{28}$$

The derivation refers to Appendix. The cross terms of the target echo and noise appear in the non-linear multiplication output. As a result, the output SNR of the proposed method is no longer proportional to the input SNR. Three situations are discussed as follows:

- *Low input SNR* $\zeta_i \ll 1$
  The input SNR is much less than 1. The output SNR $\zeta_o \approx N{\zeta_i}^2$ improves $N\zeta_i$ times compared to input SNR.
- *Input SNR* $\zeta_i \approx 1$
  The input SNR is about equal to 1. The output SNR is approximately one third of N, i.e., $\zeta_o \approx N/3$.
- *High input SNR* $\zeta_i \gg 1$
  The input SNR is much greater than 1. The output SNR $\zeta_o \approx N\zeta_i/2$ improves $N/2$ times compared to input SNR.

Taking the random phase term in Eq. (16) into consideration, an attenuation factor γ should be introduced into the formula of output SNR. The output SNR ζ_o is modified as

$$\zeta_o = \gamma N\frac{{\zeta_i}^2}{2\zeta_i + 1}. \tag{29}$$

The factor γ is determined by the modulated coefficient c_n and target velocity V_0. Using the M-sequence as the source of pseudorandom code, the factor γ is about 0.9528 under the condition of the target velocity $V_0 = 20$ m/s. It implies that the SNR loss caused by the neglect of random phase term is about 0.42 dB.

B. APPLICATION IN MULTI-TARGET SCENARIO

Then, the application of CCC algorithm is also studied in the multi-target scenario. It is assumed that the echo intensities of targets do not change with hopping frequencies. When the targets move with different velocities, the baseband sampling echoes in the adjacent complementary CPIs can be written as

$$y_{rM}[n] = \sum_{i=1}^{I}\sigma_i \exp\left(-j\frac{4\pi}{c}\left(f_0 + c_n\Delta f\right)\left(R_i + V_i nT_r\right)\right) \tag{30}$$

and

$$\hat{y}_{rM}[n] = \sum_{i=1}^{I}\sigma_i \exp\left(-j\frac{4\pi}{c}\left(f_0 + \hat{c}_{n+N}\Delta f\right)\left(R_i + V_i(n+N)T_r\right)\right) \tag{31}$$

where I indicates the number of targets.

Then, the sampling echoes are multiplied together

$$\begin{aligned}\upsilon_M[n] &= y_{rM}\cdot\hat{y}_{rM} \\ &= \sum_{p=1}^{I}\sum_{q=1}^{I}\sigma_p\sigma_q\Phi_0\Phi_V\Phi_R\Phi_{V'}\end{aligned} \tag{32}$$

where

$$\Phi_0 \triangleq \exp\left(-j\frac{4\pi}{c}f_0\left(R_p + R_q + V_q NT_r\right)\right)$$

$$\Phi_V \triangleq \exp\left(-j\frac{4\pi}{c}f_0\left(V_p + V_q\right)nT_r\right)$$

$$\Phi_R \triangleq \exp\left(-j\frac{4\pi}{c}\Delta f\left(c_n R_p + \hat{c}_{n+N}R_q\right)\right)$$

$$\Phi_{V'} \triangleq \exp\left(-j\frac{4\pi}{c}\Delta f\left(c_n V_p nT_r + \hat{c}_{n+N}V_q\left(n+N\right)T_r\right)\right)$$

In the multiplying result, Φ_0 is the constant phase term. It has little influence on the velocity profiles after using the absolute value. $\Phi_{V'}$ is the interference term whose phase is composed of the target velocity and frequency step interval. As long as the velocities are not fast or coarsely compensated,

$\Phi_{V'}$ can be neglected as a tiny phase noise. Finally, only the velocity term Φ_V and range term Φ_R are left.

The velocity term Φ_V still has the linear phase, while the range term Φ_R is the random phase term. Since multiplication is a non-linear operation, it generates I self-terms (when $p = q$) and $I(I-1)$ cross-terms (when $p \neq q$). For the self-term $R_p = R_q$, the complementary codes make the range terms cancel each other out. The range phases become the constants after multiplying, and then velocity phases can be accumulated coherently. For the cross-terms, there are two situations. In one scenario, the initial target ranges are not equal, i.e., $R_p \neq R_q$ when $p \neq q$. Their range terms Φ_R remain random. The range term forms a disturbance factor and the velocity term achieves the role of cyclic shift. After the velocity profile synthesis processing, the cross-term's energy is completely defocused. In the other scenario, two targets have the same initial range, i.e., $R_p = R_q$ when $p \neq q$. This situation is similar to the self-term. Then, a fake velocity emerges at the middle of real velocities. That is

$$V_{\text{fake}} = \frac{V_p + V_q}{2}, \quad \text{when } R_p = R_q \, (p \neq q) \, . \tag{33}$$

The fake velocity interferes with measuring target velocities, which may elicit the false velocity alarm.

The procedure utilizing CCC algorithm in RSF radars to detect the moving targets is summarized in **Algorithm 2**.

Algorithm 2 The CCC Algorithm Utilized in RSF Radars

1: **Transmitting terminal**
   During the adjacent CPIs, the waveforms modulated by the complementary codes are transmitted.
2: **Quadrature sampling**
   In the receiver, the echoes are demodulated with the transmitted waveforms as LO. Then, the baseband echoes are sampled along the range dimension.
3: **Velocity Estimation**
   In each range bin, the CCC algorithm described by **Algorithm 1** is performed to estimate target velocities.
4: **Motion compensation**
   The compensation factors are generated using Eq. (22) and then multiplied with the sampling echoes to achieve the motion compensation in different velocity channels.
5: **Reordering and synthesizing the HRRP**
   The compensated echoes are reordered according to the ascending order of coefficient c_n. Then, the compensated HRRPs in different velocity channels are synthesized by performing IFFT on the reordered echoes.
6: **Subsequent processing**
   The target ranges are obtained by carrying out the detection on the compensated HRRPs. The range and velocity parameters can be fused for display, or the HRRP of the whole scenario can be integrated to facilitate the subsequent processing, e.g., classification, distinction and recognition of target, etc.

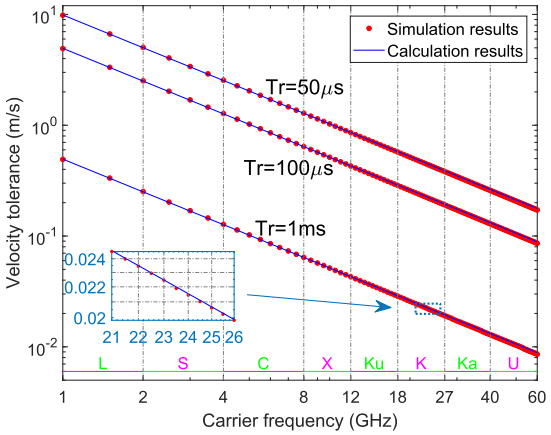

FIGURE 3. The simulated and calculated VT varies with carrier frequency f_0 under the condition of different PRIs.

TABLE 2. The parameters of simulated targets.

Target	I	II	III	IV
Amplitude	1.1	1.2	1.1	1.3
Range (km)	5.1	5	5.05	5.1
Velocity (m/s)	5	10	10	20

VI. ALGORITHM SIMULATIONS AND COMPARISONS

A. ALGORITHM SIMULATIONS

Firstly, the simulation is carried out on the velocity tolerance. Figure 3 shows the simulated and calculated VTs varying with the carrier frequency under the condition of different PRIs in the logarithmic coordinate system. Simulations cover the common radar band from 1 GHz to 60 GHz with the step of 500 MHz, i.e., from the L band to U band. In the figure, the red dots mark the raw data of simulation results, while the blue lines signify the calculated VT by Eq. (11). It can be seen that the calculated VT is coincident with the simulation result. The RSF radar always has a very small VT. As a result, the high accuracy motion compensation is necessary before synthesizing the HRRP.

Then, the CCC algorithm is simulated to demonstrate its applicability in the multi-target scenario. The simulated radar parameters are set the same as those in Figure 2. In addition, four targets with different ranges and velocities listed in Table 2 are utilized during the simulations. The targets are located in the same range bin, simultaneously.

The velocity profile synthesized by the CCC algorithm is shown by the blue line in Figure 4. The estimated velocities can be obtained by performing the CFAR detection on this velocity profile. The red line in Figure 4 denotes detection threshold. Then, a set of compensation factors can be generated via Eq. (22). Subsequently, these compensation factors should be multiplied with the sampling echoes to achieve the motion compensation. Finally, the HRRPs of targets are synthesized by performing an IFFT on the compensated echoes.

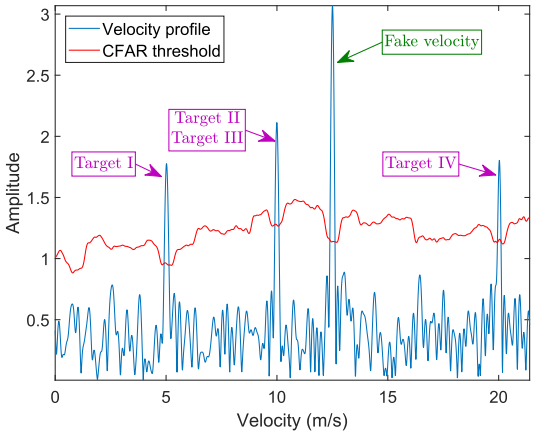

FIGURE 4. The velocity profile of simulated multi-target scenario described in Tabble 2 (blue line) and its CFAR threshold (red line) *versus* the velocity within a unambiguous velocity interval.

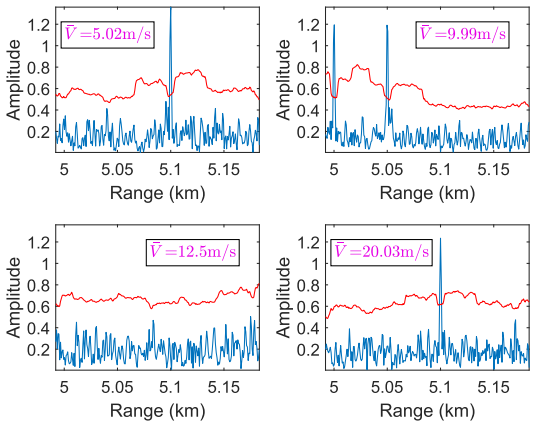

FIGURE 5. The compensated HRRP using the estimated velocities of Figure 4 (blue lines) and its CFAR threshold (red lines) *versus* the range in km. Parameter $\bar{V}$ in each subfigure represents the estimated velocity value.

After the velocity estimation, four velocity channels are obtained. The compensated HRRPs in these velocity channels are shown in Figure 5. The HRRP can be coherently accumulated only if there are targets located in the current velocity channel. The peaks in the HRRPs accurately reflect target ranges. In contrast, the powers of other targets are dispersed over the range bin in the current velocity channel. Moreover, the compensated HRRP is also defocused in the fake velocity channel, because the differences between the fake velocity and target velocities are all greater than VT.

Similarly, the target ranges can be obtained by performing detection on the compensated HRRP. After the target velocities and ranges are estimated, two-dimensional target parameters can be fused, which are displayed in Figure 6. In addition, the estimated values and estimation errors are also collected in Table 3.

The estimated values restore the ranges and velocities of the simulated targets in Table 2. The range and velocity estimation errors are all less than half of the range resolution and VT, i.e., 0.75 m and 0.7389 m/s, respectively. Therefore, the

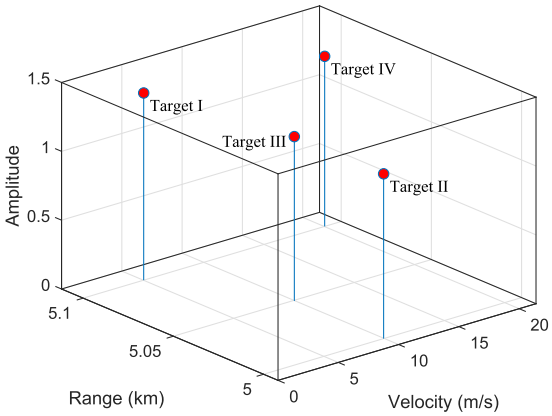

FIGURE 6. The fusion figure of estimated velocity and range parameters. The velocities and ranges are detected from Figure 4 and 5, respectively.

TABLE 3. The estimated parameters and absolute errors.

Target		I	II	III	IV
Amplitude	Real	1.1	1.2	1.1	1.3
	Estimated	1.25	1.20	1.19	1.24
	Error	0.15	0	0.09	0.06
Range (km)	Real	5.1	5	5.05	5.1
	Estimated	5.100	5.00025	5.04975	5.100
	Error	0	0.00025	0.00025	0
Velocity (m/s)	Real	5	10	10	20
	Estimated	5.0176	9.9934	9.9934	20.0286
	Error	0.0176	0.0064	0.0064	0.0286

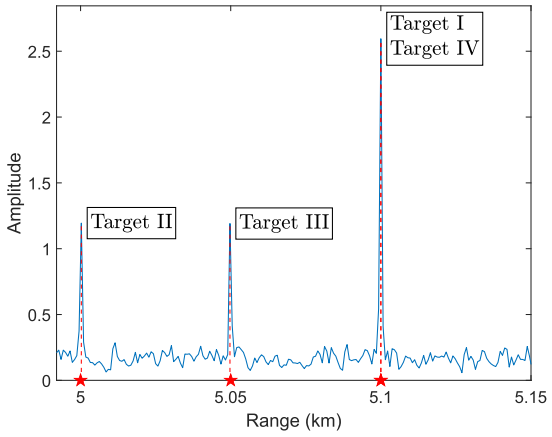

FIGURE 7. The synthetic HRRP of simulated scenario integrated with the range profile in each velocity channel shown in Figure 5 *versus* the range in km. The red stars on x-axis mark the ranges of targets.

CCC algorithm is capable of detecting the ranges and velocities of multiple targets for RSF radars.

Furthermore, if the HRRP of whole scenario is required, the following method is recommended. Based on the detection result on the compensated HRRP, several targets may be detected in the same fine range bin. The profiles of these targets should be added together, while the profiles at other places should be averaged. In this way, the signal energies of targets are enhanced, while the energies of side-lobes and noise are smoothed. Figure 7 shows the synthetic

TABLE 4. The comparison of different compensation methods.

Method	Ap.	Ac.	UVI	C.C.	M.T.	CPI
HT-TSS	*N*	–	–	*H*	*N*	Many
RFRFT	*N*	–	–	*H*	*Y*	Many
RLVD	*N*	–	–	*H*	*Y*	Many
TFD	*N*	–	–	*H*	*Y*	1
CC-TAP	*Y*	*C*	*L*	*S*	*N*	2
DFs	*Y*	*P*	*L*	*H*	*Y*	1
MWE	*Y*	*P*	*L*	*H*	*N*	1
RV-IAP	*Y*	*P*	*L*	*H*	*Y*	1
CCC	***Y***	***P***	***S***	***S***	***Y***	**2**

[1]Ap. = applicability, represents the applicability of the method to achieve motion compensation for RSF radars. *N* = no, *Y* = yes.
[2]Ac. = accuracy, represents the accuracy level of the compensation method. *P* = high-accuracy, *C* = coarse accuracy.
[3]UVI = unambiguous velocity interval. *L* = large, *S* = small.
[4]C.C. = computation complexity. *H* = high, *S* = small.
[5]M.T. = multiple targets, indicates whether the method is capable of detecting multiple targets with different velocities. *N* = no, *Y* = yes.
[6]CPI = coherent processing interval, indicates how many CPIs the method needs to achieve motion compensation.

HRRP integrated from the compensated range profile in each velocity channel. The peaks in HRRP can accurately reflect the target ranges. The profiles of Target I and IV are added together because they are located at the same fine range bin.

B. METHOD COMPARISONS

Several methods have been referred to achieve the motion compensation for HRRP radars. At last, the CCC algorithm is compared with these methods to highlight its advantages and shortcomings. Table 4 summarizes the characteristics of these methods when applied to RSF radars.

The HT-TSS and TFD methods were proposed to achieve the motion compensation for LSF radars. Before the motion compensation, the HRRP can still be synthesized in spite of a little quality deterioration. The strong scatterers can be tracked and the Hough transform can make use of HRRPs in several CPIs for LSF radars to improve the robustness of velocity estimation. However, the HRRP of moving target is defocused before motion compensation in RSF radars, which makes the strong scatterers difficult to be tracked. The TFD method measures the parameters of the regular distribution curve on the time-frequency plane for LSF radars to obtain the target range and velocity. Due to the defocusing coupling effect between the echo delay and Doppler frequency, the TFD curve of RSF radar echo is irregular. It is difficult to extract the velocity and range parameters from the irregular TFD curve. The RFRFT and RLVD methods estimate the target range, velocity and acceleration by coherently accumulating the target's energy into a peak in the time-range plane for LFM radars. However, the pulse-compressed signal of maneuvering target with constant acceleration cannot be modeled as a LFM signal in RSF radars. Furthermore, the HRRP in each CPI are divergent before motion compensation. Therefore, the HT-TSS, TFD, RFRFT, and RLVD methods are not applicable for RSF radars to achieve the velocity estimation.

TABLE 5. The velocity estimation accuracies of different methods.

	CC-TAP	DFs	MWE	RV-IAP	CCC
Accuracy (m/s)	51.8	0.148	0.148	< 0.148	0.074

The CC-TAP method uses the correlation of the uncomensated HRRPs in two CPIs to estimate the target velocity. In [37], it has been deduced that the compensation accuracy is inversely proportional to the synthetic bandwidth. However, the compensation accuracy of RSF radar, i.e., VT, is limited by carrier frequency. The carrier frequency is always much greater than the synthetic bandwidth. As a result, the CC-TAP method cannot satisfy the requirements of motion compensation accuracy in RSF radars. But it can be applied as a coarse velocity estimation method before using CCC algorithm to enlarge the unambiguous velocity interval.

The DFs and MWE method have the similar characteristics of enumerating all possible velocity channels. The DFs method sets a series of Doppler filters, while the MWE method compares the waveform entropy of the HRRPs under conditions of different compensating velocities. If the target velocity is not known in advance, the enumeration has to be conducted on a wide search interval. A high velocity estimation accuracy is always needed in RSF radars. Consequently, the DFs method requires lots of hardware resources and the MWE method requires lots of iteration time, indicating that both methods have high computation complexity.

Based on the sparsity of target in the HRRP, the RV-IAP method is capable of detecting the ranges and velocities of multi-targets. It is a kind of iterative projection method. However, its convergence condition relies on the number of targets. Thus, the number of targets should be estimated as as the prior knowledge before performing the RV-IAP method. In addition, the projection involves lots of matrix inversion operation. As a result, its computation complexity grows exponentially as the number of targets increases.

As for the CCC method proposed in this paper, its velocity estimation accuracy is sufficient to achieve the motion compensation for RSF radars. The estimation accuracy is only half of the VT, which makes the signal attenuation that is caused by the velocity estimation error less than 0.71 dB. The false velocity alarm may arise when detecting multiple targets. But the fake velocity has no influence on synthesizing the complete HRRP owing to the thumbtack range-velocity ambiguity function. Moreover, the method can be fast implemented by IFFT. As a result, the computation complexity of the proposed method is $O\left(N \log_2 N\right)$ which is the smallest among these methods. Finally, the proposed method can also achieve the range-velocity estimation for multiple targets.

Table 5 lists the velocity estimation accuracies of different methods. The simulating parameters are set as follows: the

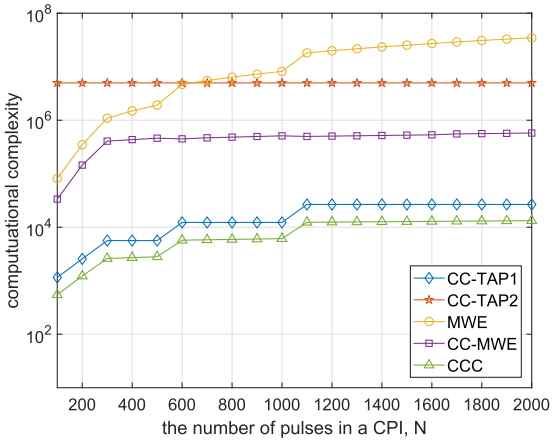

FIGURE 8. The computation complexities of different velocity estimation methods *versus* the number of pulses in a CPI *N*. CC-TAP1 denotes the CC-TAP method with the original correlation step, while CC-TAP2 denotes the CC-TAP method with the shrunk correlation step. The proposed CCC method has the lowest computation complexity.

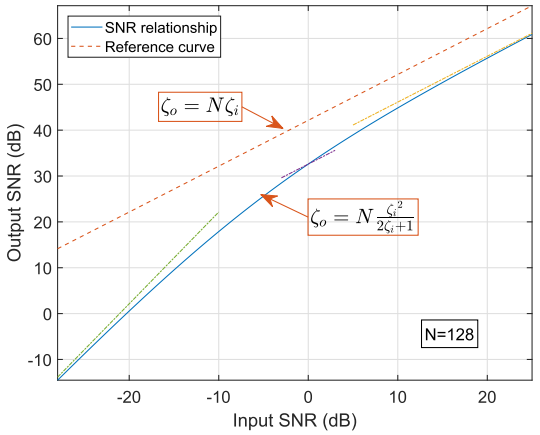

FIGURE 9. The relationship between output SNR and input SNR in dB. The point lines near SNR relationship curve denote the progressive lines at low, moderate and high SNRs which corresponds to the discussions in Sec. V-A.3.

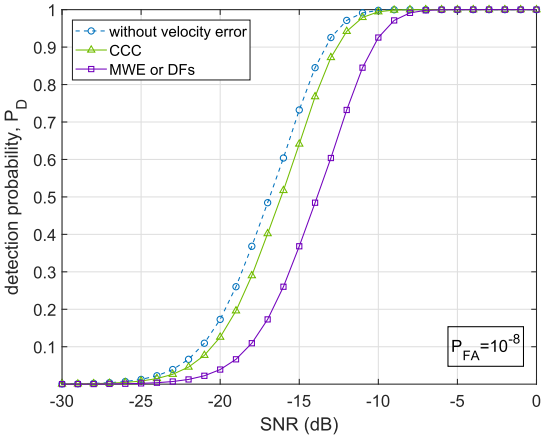

FIGURE 10. The detection probabilities of target based on the HRRPs compensated by different methods *versus* the input SNR with the false alarm probability $P_{FA}=10^{-8}$.

carrier frequency $f_0 = 35$ GHz, synthetic bandwidth $B = 100$ MHz, $N = 128$, PRI $T_r = 100\ \mu s$ and pulse duration $T = 1\ \mu s$. The estimation accuracy of CC-TAP method determined by the synthetic bandwidth is much greater than VT $v_T = 0.148$ m/s. The search step of DFs and MWE methods have to be limited to v_T to make the attenuation of the compensated HRRP less than 3 dB. Referring to [28], the RV-IAP method is capable of distinguishing two targets with the accuracy less than v_T. Meanwhile, the CCC method also has a high estimation accuracy that is just half of VT.

The computation complexity is defined as the number of the complex multiplications during the velocity estimation in one range bin. Figure 8 shows the computation complexity of the proposed CCC method compared to that of the existing methods. In the simulations, the number of pulses in a CPI, i.e., N, increases from 100 to 2000 and the frequency step interval is $\Delta f = 1$ MHz. The CC-TAP1 in Figure 8 denotes the coarse motion compensation method introduced by [18], while the CC-TAP2 is the shrunk correlation step version of CC-TAP method to make the compensation accuracy satisfy the requirements of RSF radars [37]. The search boundary of MWE method is set to the unambiguous velocity interval of CCC method, and the search step is set to VT. The CC-MWE combines CC-TAP1 and MWE methods; specifically, it first achieves the coarse velocity estimation by CC-TAP1, and then achieve the precise estimation by MWE. Although CC-TAP1 possesses the similar computation complexity to the proposed method, its estimation accuracy is too coarse to satisfy the compensation requirements. The computation complexity of MWE method is $O\left(N^2 \log_2 N\right)$ which grows fastest. While, the computation complexity of CCC method described by Eq. (26) is lowest in Figure 8. Therefore, the proposed method can significantly reduce the computation complexity and preserve the estimation performance.

The relationship between the output and input SNR of CCC method is shown by the blue solid line in Figure 9. The output SNR is not proportional to the input SNR due to the non-linear multiplication. Compared with the case of high input SNR, the output SNR improves less at the low input SNR. However, the output SNR can still be amplified by increasing N in the situation of low input SNR to preserve the velocity estimation accuracy.

Furthermore, the target can be detected on the compensated HRRP. However, these compensated methods may cause different SNR loss in the HRRP, which affects the target detection probability. It is assumed that the compensated velocities have the maximum estimation error. The estimation error of both MWE and DFs methods are VT which attenuates the compensated HRRP of target by 3 dB. However, the maximal attenuation of the HRRP compensated by CCC method is only 0.71 dB. As a result, the SNRs of the compensated HRRPs by these methods are different, which brings about the different detection probabilities of targets,. The detection probabilities on the HRRPs compensated by the these methods are shown in Figure 10 with the false alarm probability $P_{\mathrm{FA}} = 10^{-8}$. The blue dashed line also plots the

detection probability without the velocity estimation error as a reference. It can be seen that high velocity compensation accuracy is capable of significantly improving target detection probability on the HRRP.

The CCC method also has shortcomings. Firstly, the unambiguous velocity interval is sacrificed in exchange for the high estimation accuracy. Therefore, it is necessary to conduct a coarse motion compensation to prevent the ambiguous errors before performing the CCC method when detecting the fast-moving targets. Then, the complex multiplication is a nonlinear operation. When addressing the multi-target scenario, the cross-terms may raise the side-lobes of velocity profiles. Accordingly, we hope to design the novel side-lobe suppression method for CCC method to improve the multi-target detection performance in our future work.

VII. CONCLUSIONS

In the paper, the RSF radar modulated by the M-sequence-type code is first provided. M-sequence is widely applied to approximate white noise. The code generated by M-sequence inherits its outstanding pseudorandom characteristics which makes the RSF radar have an ideal thumbtack-type ambiguity function.

In RSF radars, the HRRP is very sensitive to the target velocity. A small target movement can completely destroy the HRRP, called the defocusing coupling effect. Consequently, the velocity estimation and compensation should be performed before synthesizing the HRRP for RSF radars. The CCC algorithm is proposed in the paper to estimate the target velocity and achieve motion compensation. The algorithm idea is adopting the complementary pseudorandom codes to modulate the transmitted waveforms in two adjacent CPIs to separate the range and velocity terms of sampling echoes. The algorithm can be efficiently implemented by IFFT processing. The performance analyses demonstrate that the proposed algorithm is capable of obtaining the high estimation accuracy and improving SNR with the low computation complexity. Simulation results further validate the effectiveness and efficiency of the proposed algorithm.

APPENDIX

OUTPUT SNR OF CCC ALGORITHM

Let $x[n] = \sigma \exp\left(-j4\pi\left(f_0+c_n\Delta f\right)\left(R_0+V_0nT_r\right)/c\right)$ be the sampling echo of point target. The echo model in Eq. (6) can be rewritten as

$$y_r[n] = x[n] + w[n] \tag{34}$$

where $w[n]$ is the zero-mean and ε-variance additive white Gaussian noise. The complementary echo is also rewritten as

$$\hat{y}_r[n] = \hat{x}[n] + \hat{w}[n]. \tag{35}$$

The input SNR can be obtained as

$$\zeta_i = \frac{\mathrm{E}^2\{y_r[n]\}}{\mathrm{var}\{y_r[n]\}} = \frac{\sigma^2}{\varepsilon} \tag{36}$$

where $\mathrm{E}\{\}$ and $\mathrm{var}\{\}$ denote to calculate the mathematical expectation and variance of random variable, respectively.

The echoes in the adjacent CPIs are multiplied

$$\begin{aligned}\upsilon[n] &= y_r[n]\cdot\hat{y}_r[n] \\ &= x\hat{x} + x\hat{w} + \hat{x}w + w\hat{w}.\end{aligned} \tag{37}$$

Noise terms $x\hat{w}$, $\hat{x}w$, and $w\hat{w}$ are independent of each other. The mathematical expectation of $\upsilon[n]$ is

$$\mathrm{E}\{\upsilon[n]\} = x\hat{x}. \tag{38}$$

And the variance of $\upsilon[n]$ is

$$\mathrm{var}\{\upsilon[n]\} = \mathrm{var}\left\{x\hat{w} + \hat{x}w + w\hat{w}\right\} = 2\sigma^2\varepsilon + \varepsilon^2. \tag{39}$$

The velocity profile is obtained by performing the IDFT on the multiplying result. That is

$$\Upsilon[q] = \frac{1}{N}\sum_{n=0}^{N-1}\upsilon[n]\exp\left(j2\pi\frac{nq}{Q}\right) \tag{40}$$

Neglecting the influence of the random phase term and considering the velocity profile in Eq. (19), the output SNR at $q_0 = 2\left(2f_0+N\Delta f\right)V_0T_rK/c$ is

$$\begin{aligned}\zeta_o &= \frac{\left|\mathrm{E}\{\Upsilon[q_0]\}\right|^2}{\mathrm{var}\{\Upsilon[q_0]\}} = \frac{\left|\frac{\sigma^2}{N}\sum_{n=0}^{N-1}\mathrm{E}\{\upsilon[n]\}\exp\left(j2\pi\frac{nq_0}{Q}\right)\right|^2}{\frac{1}{N^2}\sum_{n=0}^{N-1}\mathrm{var}\{\upsilon[n]\}} \\ &= \frac{N\sigma^4}{2\sigma^2\varepsilon+\varepsilon^2} = N\frac{{\zeta_i}^2}{2\zeta_i+1}.\end{aligned} \tag{41}$$

REFERENCES

[1] M. Y. Chua, V. C. Koo, H. S. Lim, and J. T. S. Sumantyo, "Phase-coded stepped frequency linear frequency modulated waveform synthesis technique for low altitude ultra-wideband synthetic aperture radar," *IEEE Access*, vol. 5, pp. 11391–11403, 2017.

[2] T. Lane, "Stepped-frequecny and ISAR imaging systems," in *Coherent Radar Performance Estimation*, J. A. Scheer and J. L. Kurtz, Eds. Norwood, MA, USA: Artech House, 1993, ch. 11.

[3] X. Pan *et al.*, "Extraction of micro-Doppler frequency from HRRPs of rotating targets," *IEEE Access*, vol. 5, pp. 26162–26174, 2017.

[4] J. E. S. Fransson, F. Walter, K. Blennow, A. Gustavsson, and L. M. H. Ulander, "Detection of storm-damaged forested areas using airborne CARABAS-II VHF SAR image data," *IEEE Trans. Geosci. Remote Sens.*, vol. 40, no. 10, pp. 2170–2175, Oct. 2002.

[5] T. Long, Y.-Q. Han, and E.-K. Mao, "Digital signal processing of stepped frequency radar," *Acta Aeronaut. Astronaut. Sin.*, vol. 22, pp. S16–S25, Jun. 2001.

[6] N. Levanon and E. Mozeson, *Radar Signals*. New York, NY, USA: Wiley, 2004.

[7] S. R. J. Axelsson, "Noise radar using random phase and frequency modulation," *IEEE Trans. Geosci. Remote Sens.*, vol. 42, no. 11, pp. 2370–2384, Nov. 2004.

[8] S. R. J. Axelsson, "Analysis of random step frequency radar and comparison with experiments," *IEEE Trans. Geosci. Remote Sens.*, vol. 45, no. 4, pp. 890–904, Apr. 2007.

[9] P. Liu, W. Qi, Y. Zhang, and L. Wei, "On the unambiguous distance of multicarrier phase ranging with random hopped frequencies," *IEEE Access*, vol. 5, pp. 10296–10306, 2017.

[10] M. C. Shastry, R. M. Narayanan, and M. Rangaswamy, "Sparsity-based signal processing for noise radar imaging," *IEEE Trans. Aerosp. Electron. Syst.*, vol. 51, no. 1, pp. 314–325, Jan. 2015.

[11] C. Wasserzier and G. Galati, "Advanced range-Doppler processing in noise radar," in *Proc. 22nd Int. Microw. Radar Conf. (MIKON)*, 2018, pp. 464–467.
[12] Y. Zhang, Y. Li, L. Jin, and M. Gao, "Sensitivity of cancellation algorithm to transmitted waveform in noise radar system," in *Proc. 12th Int. Conf. Signal Process. (ICSP)*, 2014, pp. 246–251.
[13] Z. Liao, D. Lu, J. Hu, and J. Zhang, "A novel range profile synthesis method for random hopping frequency radar," in *Proc. IEEE Digit. Signal Process. Conf. (DSP)*, Oct. 2016, pp. 79–83.
[14] X. Chen, J. Guan, Y. He, and X. Yu, "High-resolution sparse representation and its applications in radar moving target detection," *J. Radars*, vol. 6, no. 3, pp. 239–251, 2017.
[15] S. W. Golomb and H. Taylor, "Constructions and properties of Costas arrays," *Proc. IEEE*, vol. 72, no. 9, pp. 1143–1163, Sep. 1984.
[16] J. P. Costas, "A study of a class of detection waveforms having nearly ideal range—Doppler ambiguity properties," *Proc. IEEE*, vol. 72, no. 8, pp. 996–1009, Aug. 1984.
[17] Y. Zhang, W. Hu, L. Wang, and L. Zhang, "A novel random stepped frequency radar using Chaos," in *Proc. IEEE Radar Conf.*, May 2014, pp. 0663–0665.
[18] T. Huang, Y. Liu, G. Li, and X. Wang, "Randomized stepped frequency ISAR imaging," in *Proc. IEEE Radar Conf.*, Apr. 2012, pp. 0553–0557.
[19] T. Sauer and A. Schroth, "Robust range alignment algorithm via Hough transform in an ISAR imaging system," *IEEE Trans. Aerosp. Electron. Syst.*, vol. 31, no. 3, pp. 1173–1177, Jul. 1995.
[20] G. Y. Delisle and H. Wu, "Moving target imaging and trajectory computation using ISAR," *IEEE Trans. Aerosp. Electron. Syst.*, vol. 30, no. 3, pp. 887–899, Jul. 1994.
[21] R. Xu, Z. Cao, and Y. Liu, "Method of precise motion compensation for ISAR," *Proc. SPIE*, vol. 1152, pp. 288–295, Nov. 1989.
[22] R. Xu, Z. Cao, and Y. Liu, "Motion compensation for ISAR and noise effect," *IEEE Aerosp. Electron. Syst. Mag.*, vol. 5, no. 6, pp. 20–22, Jun. 1990.
[23] C.-C. Chen and H. C. Andrews, "Target-motion-induced radar imaging," *IEEE Trans. Aerosp. Electron. Syst.*, vol. AES-16, no. 1, pp. 2–14, Jan. 1980.
[24] N. Levanon, "Stepped-frequency pulse-train radar signal," *IEE Proc.-Radar, Sonar Navigat.*, vol. 149, no. 6, pp. 297–309, Dec. 2002.
[25] X. Li, G. Liu, and J. Ni, "Autofocusing of ISAR images based on entropy minimization," *IEEE Trans. Aerosp. Electron. Syst.*, vol. 35, no. 4, pp. 1240–1252, Oct. 1999.
[26] Z. Liu and S. Zhang, "A novel method of translational motion compensation for hopped-frequency ISAR imaging," in *Proc. IEEE Int. Radar Conf.*, May 2000, pp. 255–260.
[27] P. Song, H. Meng, T. Huang, and Y. Liu, "A novel target motion compensation method for randomized stepped frequency ISAR," in *Proc. Asilomar Conf. Signals, Syst. Comput.*, 2013, pp. 917–921.
[28] Y. Liu, H. Meng, G. Li, and X. Wang, "Range-velocity estimation of multiple targets in randomised stepped-frequency radar," *Electron. Lett.*, vol. 44, no. 17, pp. 1032–1034, Aug. 2008.
[29] A. Yasotharan and T. Thayaparan, "Time-frequency method for detecting an accelerating target in sea clutter," *IEEE Trans. Aerosp. Electron. Syst.*, vol. 42, no. 4, pp. 1289–1310, Oct. 2006.
[30] A. Yasotharan and T. Thayaparan, "Optimum time–frequency distribution for detecting a discrete-time chirp signal in noise," *IEE Proc.-Vis., Image Signal Process.*, vol. 153, no. 2, pp. 132–140, Apr. 2006.
[31] Y. Wang, H. Ling, and V. C. Chen, "ISAR motion compensation via adaptive joint time-frequency technique," *IEEE Trans. Aerosp. Electron. Syst.*, vol. 34, no. 2, pp. 670–677, Apr. 1998.
[32] X. Chen, J. Guan, N. Liu, and Y. He, "Maneuvering target detection via Radon-fractional Fourier transform-based long-time coherent integration," *IEEE Trans. Signal Process.*, vol. 62, no. 4, pp. 939–953, Feb. 2014.
[33] X. Chen, F. Cai, Y. Cong, and J. Guan, "Radon-fractional Fourier transform and its application to radar maneuvering target detection," in *Proc. Int. Conf. Radar*, 2013, pp. 346–350.
[34] X. Chen, J. Guan, X. Li, and Y. He, "Effective coherent integration method for marine target with micromotion via phase differentiation and Radon-Lv's distribution," *IET Radar Sonar Navigat.*, vol. 9, no. 9, pp. 1284–1295, 2015.
[35] X. Li, G. Cui, W. Yi, and L. Kong, "Coherent integration for maneuvering target detection based on Radon-Lv's distribution," *IEEE Signal Process. Lett.*, vol. 22, no. 9, pp. 1467–1471, Sep. 2015.
[36] M. A. Richards, *Fundamentals of Radar Signal Processing*. New York, NY, USA: McGraw-Hill, 2005.
[37] Z. Liao, J. Hu, D. Lu, J. Ou, and J. Zhang, "A novel motion compensation method for random frequency hopping radar," in *Proc. IEEE 10th Int. Congr. Image Signal Process., Biomed. Eng. Inform. (CISP-BMEI)*, Oct. 2017, pp. 1–6.

ZHIKUN LIAO received the B.Eng. degree in electronic science and technology from the Beijing Institute of Technology, Beijing, China, in 2012. He is currently pursuing the Ph.D. degree with the National University of Defense Technology, Changsha, China.

His research interests include radar signal processing and automation target recognition.

JIEMIN HU was born in Anhui, China, in 1983. He received the M.S. and Ph.D. degrees from the National University of Defense Technology (NUDT), Changsha, China, in 2006 and 2011, respectively. He is currently a Lecturer with the ATR Laboratory, NUDT.

His research interests include radar signal processing, feature extraction, and radar imaging.

DAWEI LU was born in Hubei, China, in 1981. He received the M.S. degree from the National University of Defense Technology (NUDT), Changsha, China, in 2005. He is currently pursuing the Ph.D. degree in electrical engineering with NUDT.

His research interests include radar signal processing, radar imaging, and radar target recognition.

JUN ZHANG was born in Hunan, China, in 1973. He received the M.S. and Ph.D. degrees from the National University of Defense Technology (NUDT), Changsha, China, in 1998 and 2002, respectively. He is currently a Professor with the ATR Laboratory, NUDT.

His research interests include radar signal processing, radar system, and automation target recognition.